Optical Saturation as a Versatile Tool to Enhance Resolution in Confocal Microscopy

Jana Humpolíčková,[†*] Aleš Benda,[†] and Jörg Enderlein[‡]
[†]J. Heyrovský Institute of Physical Chemistry, Academy of Sciences of the Czech Republic, Prague, Czech Republic; and [‡]Third Institute of Physics, Georg-August-Universität Göttingen, Göttingen, Germany

ABSTRACT One of the most actively developing areas in fluorescence microscopy is the achievement of spatial resolution below Abbe's diffraction limit, which restricts the resolution to several hundreds of nanometers. Most of the approaches in use at this time require a complex optical setup, a difficult mathematical treatment, or usage of dyes with special photophysical properties. In this work, we present a new, to our knowledge, approach in confocal microscopy that enhances the resolution moderately but is both technically and computationally simple. As it is based on the saturation of the transition from the ground state to the first excited state, it is universally applicable with respect to the dye used. The idea of the method presented is based on a principle similar to that underlying saturation excitation microscopy, but instead of applying harmonically modulated excitation light, the fluorophores are excited by picosecond laser pulses at different intensities, resulting in different levels of saturation. We show that the method can be easily combined with the concept of triplet relaxation, which by tuning the dark periods between pulses helps to suppress the formation of a photolabile triplet state and effectively reduces photobleaching. We demonstrate our approach imaging GFP-labeled protein patches within the plasma membrane of yeast cells.

INTRODUCTION

Fluorescence microscopy represents one of the most powerful imaging techniques in molecular biology, since 1), it allows for specific labeling, and 2), compared to standard light microscopy, it is enormously sensitive, yielding high image contrast. Moreover, since fluorescence excitation is rather noninvasive, fluorescence microscopy is a perfect tool for imaging in living systems. However, as with any optical imaging technique, fluorescence microscopy is diffraction-limited in resolution, and depending on the excitation and emission wavelength used, as well as the numerical aperture of the objective, its resolution is usually on the order of several hundreds of nanometers. To break that diffraction limit, special methods have been developed: stimulated emission depletion (1) reduces the volume from which fluorescence is generated by depleting excited molecules within a ringlike region at the edges of the diffraction-limited excitation spot. The final resolution is given by the saturation level of the depleting process, i.e., by the depletion intensity. This approach has been shown to achieve up to 12 times better (2) spatial resolution in a lateral dimension. By combining it with 4Pi-microscopy by using two objectives (3), it can also be used to significantly improve the axial resolution. The price of this superior performance is an enormous technical complexity, which has until now, prevented a wider distribution of stimulated emission depletion microscopy, although recent progress in the technology may perhaps change that (4). Another set of methods is based on the precise localization of stochastically activated single fluorophores and can achieve lateral resolution of ~20 nm (5–7). Nowadays, it has been shown, even common fluorescence dyes can be utilized for this kind of photoswitching microscopy (8,9), which makes these approaches even more attractive.

A third set of techniques makes use of saturation of the transition from the ground to the first excited state and the resulting nonlinearity between excitation and fluorescence intensity. For wide-field imaging, structured (10) or patterned (11) illumination is introduced, and the information on higher resolution is deduced from higher-order harmonics that appear in the Fourier transform of the image. A similar idea was also implemented for confocal microscopes, where it is known as saturation excitation (SAX) microscopy. Instead of the spatial modulation of light, a temporally modulated excitation is applied (12,13). In theory, the resolution enhancement of both these approaches can go to infinity, although the real performance is substantially dependent on the brightness and photostability of the fluorophores used. The impact of photostability is even more crucial, since the excitation intensities have to be rather large to reach sufficient saturation.

In this article, we present an alternative to SAX microscopy that, instead of using temporal harmonic light modulation, acquires the entire saturation curve at every scanning step. The amount and order of nonlinearity is obtained from fitting of the saturation curves to a theoretical model that can be represented by an infinite Taylor series. The method is both experimentally and mathematically simple, improves both lateral and axial resolution in a similar manner, and is dye-independent. The experimentally improved resolution is moderate, but comparable with resolution using SAX microscopy. The most important benefit of the presented

Submitted June 2, 2009, and accepted for publication August 3, 2009.

Jana Humpolíčková and Aleš Benda contributed equally to this work.

*Correspondence: jana.humpolickova@jh-inst.cas.cz

Editor: Levi A. Gheber.

0006-3495/09/11/2623/7 $2.00

doi: 10.1016/j.bpj.2009.08.002

method is that it can be easily combined with triplet relaxation (T-Rex) (14,15), which helps to reduce the amount of triplet state formation, resulting in significantly reduced photobleaching.

MATERIAL AND METHODS

Confocal microscopy

The experiments were performed with a home-built optical setup based on the inverted microscope IX71 (Olympus, Hamburg, Germany). The setup differs from a standard confocal setup mainly in the detector employed, the usage of a reference beam, and the synchronization of the components. The master unit is the 3D sample scanning stage (PIMars XYZ NanoPositioner, $200 \times 200 \times 200$ μm, PI, Karlsruhe, Germany), which provides the external synchronization clock for a fast back-illuminated EMCCD camera (DU-860D-CS0- #BV iXon 128 $\times$ 128 pixels, Andor, Belfast, United Kingdom). The camera sends trigger pulses to a DAQ board (PCIe 6259, National Instruments, Austin, TX), which outputs a predefined modulation voltage to an acousto-optical tunable filter (AOTFnC-400.650, AA Optoelectronic, Orsay, France), and with TTL pulses triggers the laser (470-nm diode laser head LDH-P-C-470 with PDL800-B driver unit, PicoQuant, Berlin, Germany).

A predefined sequence of 80-ps laser pulses with a time delay of 10–20 μs between them passes through the acousto-optical tunable filter, which modulates their intensity, and is then coupled into a single-mode polarization-maintaining optical fiber (LINOS Photonics, Goettingen, Germany) for spatial mode filtering. Recollimation is done with an air-spaced objective (UPLSAPO 4X, Olympus). Before the collimated laser beam enters the back port of the microscope body, part of the light, a reference beam, is reflected with a beam splitter. The microscope itself contains the standard confocal part consisting of a z470rdc dichroic mirror (Chroma, Rockingham, VT), a water immersion objective (UPLSAPO 60$\times$, Olympus), a 50-μm pinhole placed at the focal plane of the left camera port, a recollimation lens, and an HQ515/50 bandpass emission filter (Chroma). Apart from the fluorescence light, which is focused on a small spot on the CCD, the reference beam is also focused onto a different part of the CCD. The camera is operated in a frame transfer mode, taking a single line with 3×3 binning. All the focused fluorescence falls onto one single binned pixel, the focused reference light falls onto another single binned pixel, and the rest of the chip is used for background correction. The speed of the camera and the chosen operation mode make it possible to take one frame (an intensity reading) for every scanner clock tick (5 kHz). All optomechanical components were bought from Thorlabs (Newton, NJ).

For each scanned image position, several intensity readings (one per each scanner clock tick) are made with different excitation intensities (intensity ramp). In the case of measurements on labeled latex particles, 100 intensity points were acquired, and in the case of measurements in yeast cells, only two intensity levels were used. The scheme of the pulse sequence for both measurements is visualized in Fig. 1.

Sample preparation

For construction of the Ato1p-GFP strain, GFP fluorescent tag was fused (16) to the C-terminus of the *ATO1* gene directly in the chromosome. A GFP-CaURA3 cassette was provided with its 5′-end homologous to the end of the *ATO1* gene (without a stop codon) and its 3′-end homologous to the downstream region of the *ATO1* gene. For amplification of the construct, we used A1D (5′-tat gta ctg gct cgt cca ttc cca tta cca tct act gaa agg gta atc ttt ggt gac ggt gct ggt tta-3′) and A1R (5′-aaa act act ctt ttt tat ttc aat agt tct cgt tat tag tag gtc gtc ctc tcg atg aat tcg agc tcg-3′) primers and the pKT209 (17) plasmid as a template. The constructed cassette was transformed (18) into BY4742 *Saccharomyces cerevisiae* cells. Positive transformants were selected on SD agar medium. Correct integration of the cassette was verified using the VD (5′-atg tga gca agc caa aca ag-3′) and VR (5′-cgg aga cag aaa att tgt gac-3′) primers.

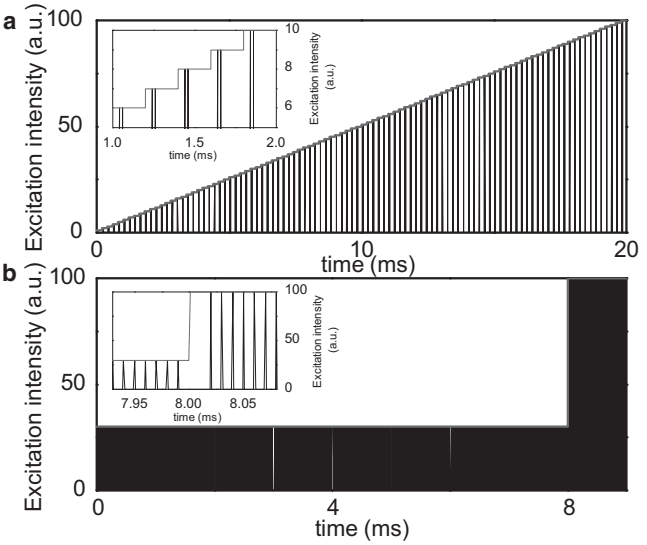

FIGURE 1 Scheme of pulsed sequences used at every pixel for bead measurements (*a*) and cell imaging (*b*). The envelope line corresponds to the intensity amplitude established on the acoustooptical tunable filter. The black peaks stand for the individual laser pulses. The insets show parts of the sequences in detail.

The live yeast cells were suspended in water and a drop of the suspension was placed on the coverslip and covered by a layer of freshly prepared agarose gel.

The 50-nm latex beads were obtained from Invitrogen (Carlsbad, CA).

THEORY

Assuming that the intersystem crossing rate is much slower than the depopulation of the S_1 state via fluorescence, at first approximation, the formation of the triplet state can be neglected and only transitions between the S_0 and the S_1 state taken into account. Then, the kinetics of S_1 formation is a solution of the equations

$$\begin{aligned} \frac{dS_0}{dt} &= -k_{ex}\, S_0 + kS_1 \\ \frac{dS_1}{dt} &= k_{ex}\, S_0 - kS_1, \end{aligned} \tag{1}$$

where S_0 and S_1 stand for the probability of finding a molecule in the S_0 and S_1 states, respectively; k is the fluorescence rate; and k_{ex} is the excitation rate during the pulses (assumed to have constant intensity over their duration), such that $k_{ex} = \sigma_{abs}\, I_{ex}\, T_R/T_p$. I_{ex} is the average excitation intensity, σ_{abs} is the absorption cross section, T_R is the time between two pulses, and T_p is the length of the pulses. For a continuous-wave excitation, $T_R = T_p$. Since we use picosecond pulses with a pulse repetition frequency low enough that all fluorophores in the S_1 state can relax to the S_0 state before the next pulse arrives, the initial conditions at the start of every excitation cycle are the same, assuming that no triplet state was formed. The saturation curve obtained from the

temporal profile of the fluorescence intensity upon excitation is (steady-state solution of Eq. 1)

$$I_{\mathrm{fl}} = kK. \tag{2}$$

K corresponds to the average probability of finding a molecule in the S_1 state during the excitation cycle. For the continuous-wave excitation, K is

$$K_{\mathrm{cw}} = \frac{\frac{k_{\mathrm{ex}}}{k}}{1 + \frac{k_{\mathrm{ex}}}{k}}; \tag{3}$$

for the pulsed excitation,

$$K_{\mathrm{pulsed}} = K_{\mathrm{cw}}\left(\frac{T_{\mathrm{p}}}{T_{\mathrm{R}}} + \frac{k_{\mathrm{ex}}}{T_{\mathrm{R}}k(k + k_{\mathrm{ex}})}\left(1 - e^{-(k+k_{\mathrm{ex}})T_{\mathrm{p}}}\right)\right). \tag{4}$$

In the continuous-wave mode, the saturation curve is described by the hyperbolic term; in the pulsed mode, saturation is governed by the exponential term in Eq. 4 (see Fig. 2). It is important to note that in the case of pulsed excitation, the excitation intensity is concentrated within the short pulses, which induces a much higher excitation rate during a pulse than the same average intensity induces in the continuous-wave mode.

On a longer timescale, the total amount of both singlet states decreases due to triplet state formation. This process occurs on a microsecond timescale. To include this triplet state formation in the model, the set of equations comprising Eq. 1 can be solved using the initial condition $\vec{s}_{t=0} = \vec{s}(\tau)$, which changes on the microsecond timescale τ. In particular, one has $S_0(t = 0) = \alpha(\tau)$ and $S_1(t = 0) = 0$. The solution of the Eq. 1 equations for S_1 then reads

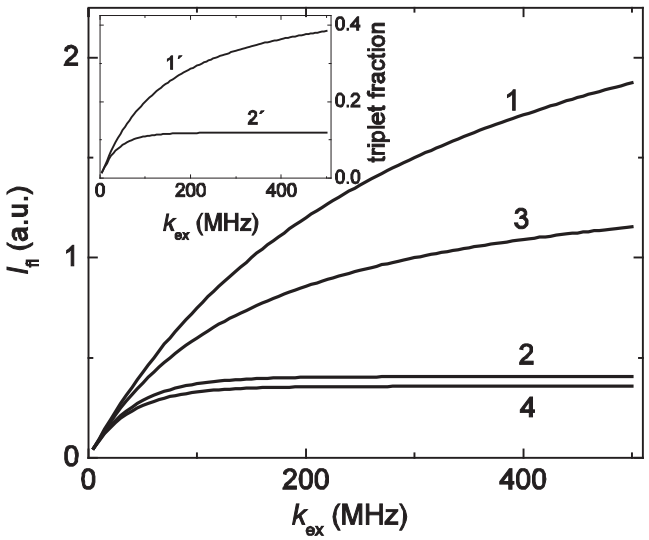

FIGURE 2 Calculated saturation curves for the dye with no transition to the triplet state for continuous-wave (*1*) and pulsed (*2*) excitation and for a dye with intersystem crossing to the triplet state for continuous-wave (*3*) and pulsed (*4*) excitation. (*Inset*) Corresponding fraction of triplet state occupancy at continuous-wave (*1′*) and pulsed (*2′*) excitation. For the calculation, the parameter values used were $\tau = \frac{1}{k} = 3$ ns, $\frac{k_{\mathrm{isc}}}{k_{\mathrm{ph}}} = 1$, $T_{\mathrm{R}} = 25$ ns, and $T_{\mathrm{p}} = 80$ ps.

$$S_1 = \frac{\alpha(\tau)\frac{k_{\mathrm{ex}}}{k}}{1 + \frac{k_{\mathrm{ex}}}{k}}\left(1 - e^{-(k+k_{\mathrm{ex}})t}\right). \tag{5}$$

The probability of finding a molecule in the triplet state is determined by $T(\tau) = 1 - S_0 - S_1 = 1 - \alpha(\tau)$. The function $\alpha(\tau)$ is a solution to the kinetic equation for the triplet state formation:

$$\frac{dT(\tau)}{d\tau} = k_{\mathrm{ISC}}\langle S_1\rangle_t - k_{\mathrm{ph}}T(\tau), \tag{6}$$

where k_{ISC} is the intersystem crossing rate and k_{ph} is the rate of phosphorescence. The angled brackets stand for the temporal average over the excitation cycle. In our case, $\langle S_1\rangle_t = \alpha(\tau)K$. The solution of Eq. 6 reads

$$\alpha(\tau) = \frac{k_{\mathrm{ph}} + k_{\mathrm{ISC}}Ke^{-(k_{\mathrm{ph}}+k_{\mathrm{ISC}}K)\tau}}{k_{\mathrm{ph}} + k_{\mathrm{ISC}}K}. \tag{7}$$

Thus, the saturation curve accounting for the triplet state formation is

$$I_{\mathrm{fl}} = \frac{kK}{1 + K\frac{k_{\mathrm{ISC}}}{k_{\mathrm{ph}}}}. \tag{8}$$

If we use Eq. 3, we obtain the saturation curve for the continuous-wave mode:

$$I_{\mathrm{fl}} = \frac{k_{\mathrm{ex}}}{1 + \frac{k_{\mathrm{ex}}}{k}\left(1 + \frac{k_{\mathrm{ISC}}}{k_{\mathrm{ph}}}\right)}. \tag{9}$$

Fig. 2 shows four saturation curves at four different conditions: pulsed and continuous excitation with and without triplet state formation. It is obvious that in the case of the pulsed excitation, the saturation behavior gets more pronounced even at lower excitation power. Moreover, in the pulsed mode, the fraction of molecules in the triplet state can be considerably reduced, since triplet state relaxes back to the ground state during the dark period.

The steady-state amount of the triplet state is given by

$$T\left(\tau >> \frac{1}{k_{\mathrm{ph}} + k_{\mathrm{isc}}K}\right) = \frac{k_{\mathrm{isc}}K}{k_{\mathrm{ph}} + k_{\mathrm{isc}}K}, \tag{10}$$

which, together with Eq. 4, relates the entire triplet state fraction with the length of the pulses (''on'' times) when the triplet state is being populated, and with the length of the dark period (''off'' times) when depopulation is occurring. Fig. 3 shows how the ratio between on and off times affects the triplet state occupancy. It is obvious that the longer the off times and the shorter the on times, the lower the amount of triplet state occupied, even at high excitation rates. It has been shown that this can be utilized for efficient suppressing of photobleaching, which mainly occurs from the triplet state (14).

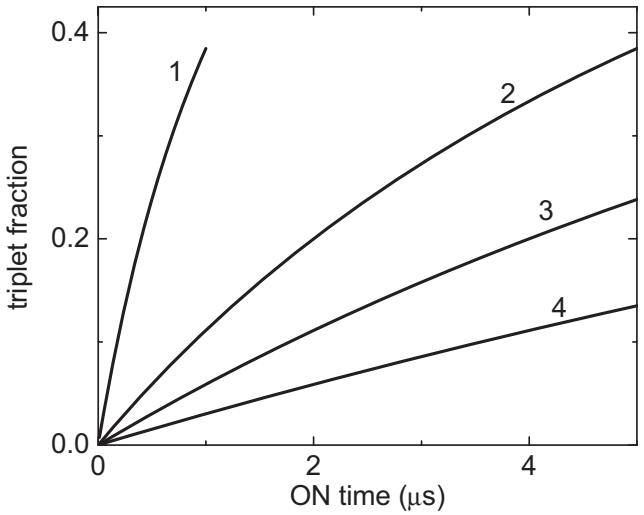

FIGURE 3 Dependence of the triplet state occupancy on pulse length (*ON time*) for repetition frequencies of 1 MHz (*1*), 200 kHz (*2*), 100 kHz (*3*), and 50 kHz (*4*). The dependencies use the excitation intensity $k_{ex} = 500$ MHz. The other parameters are the same as in Fig. 2.

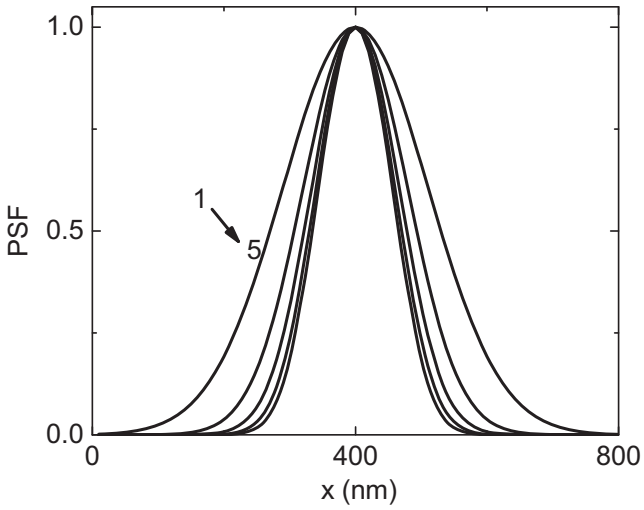

FIGURE 4 Line profiles of the contributions to the fluorescence intensity profile proportional to the first to fifth powers (*1*–*5*) of the excitation intensity in the confocal diffraction-limited spot with radius 220 nm.

The main advantage of acquiring saturation curves at every pixel of the image is that we can easily choose the scenario of the saturation and consequently keep the amount of triplet state under control. By tuning the dark periods between individual pulses, the formation of the triplet state can be almost circumvented, which allows for measuring even at powers where photobleaching would usually be unavoidable. The advantage of this approach is that it does not require any special photophysical properties of the used dye and is therefore rather universal. In all the cases described in this work, we used 80-ps pulses separated by either 10 or 20 μs, which means that the triplet state can be entirely neglected and the saturation can be described as if no triplet state was involved.

As mentioned, saturation in the pulsed mode is governed by the exponential term, which can be developed into the Taylor series:

$$I_{fl}(\vec{r}) \propto \left(1 - e^{-k_{ex}(\vec{r})*T_P}\right) = a(\vec{r})I_{ex} - b(\vec{r})I_{ex}^2 + c(\vec{r})I_{ex}^3 - d(\vec{r})I_{ex}^4 + \ldots . \quad (11)$$

Thus, the fluorescent image is composed of a sum of contributions proportional to increasing powers of the excitation intensities. The resolution of the contribution proportional to the nth power of the excitation intensity increases proportionally to $\sqrt{n}$. Fig. 4 shows line profiles of the contributions of different powers of the excitation intensity.

RESULTS AND DISCUSSION

Although there is no theoretical limit in resolution improvement, the experimentally achievable resolution is limited by the signal/noise ratio. According to Eq. 11, the saturation curves measured at every pixel have to be fitted to the higher-order polynomial functions. The fitting is more sensitive to noise the higher the used polynomial order. We tested the method by scanning subdiffractional (50 nm) heavily labeled latex particles that were deposited on a coverslip. Fig. 5 shows saturation curves at various positions within the focal spot. It is obvious that the higher the intensity, the bigger the extent of the observed saturation due to the increasing number of nonlinear terms contributing to the curve.

The saturation curves at every pixel were initially fitted to a polynomial function of the fourth order. However, in the

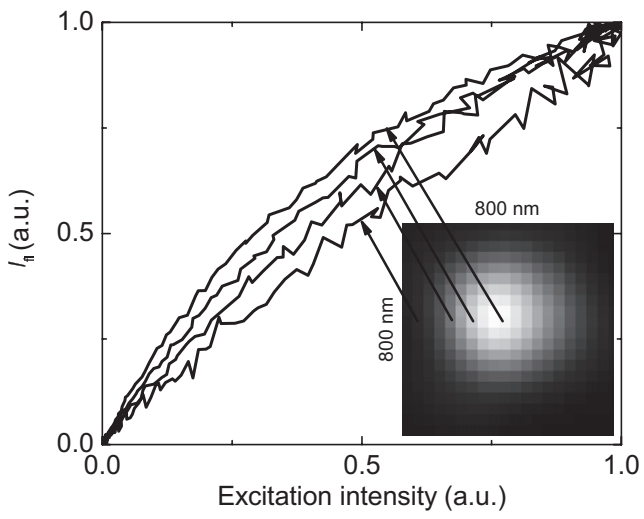

FIGURE 5 Saturation curves at different positions of the 50-nm latex particle with respect to the confocal spot. The maximum intensity (at the back aperture of the objective) of the 80-ps, 470-nm pulsed laser at 10 MHz was 60 μW. Every intensity point was generated by two pulses separated by 20 μs (see Fig. 1 *a*). The original image was 80 $\times$ 80 pixels, at 10 nm each; the image shown and the corresponding curves were obtained by 4 $\times$ 4 binning.

case of the contribution corresponding to the fourth power of the excitation intensity, the image was already too noisy to see improved resolution. Therefore, we restricted fitting to the third order, which provided us with enough signal. Fig. 6 shows the fluorescence intensity contributions corresponding to the first, second, and third powers of excitation intensity, respectively. By fitting a two-dimensional Gaussian distribution to the bead images, we determined a reduction in resolution by a factor of 1.2 for the second order and a factor of 1.3 for the third order in each direction. The discrepancy between these values and the theoretical values of 1.4 and 1.7 is due first to the noise and second to the third-order polynomial function being only a rough approximation of the entire Taylor series.

Since we obtain a reasonable improvement in resolution only for the contributions corresponding to the second and third powers of the excitation intensity, there is apparently no need to acquire the entire saturation curve. As long as the overall number of photons remains the same, two or three intensity points are sufficient. The red curve in Fig. 6 was calculated from two intensity points only. The points were obtained from the saturation curves measured at every pixel (see Fig. 5) by integrating the intensity of the first and second 50 intensity points. Apparently, resolution enhancement is almost the same, as it was obtained for the quadratic contribution from the fitting of the entire saturation curve.

In the case of cell imaging, we usually deal with fluorescent proteins that are much dimmer than the heavily labeled latex beads. Therefore, the main issue of these measurements is how many photons can be obtained at each pixel. In the case of yeast cells, we acquired signal for two intensity levels

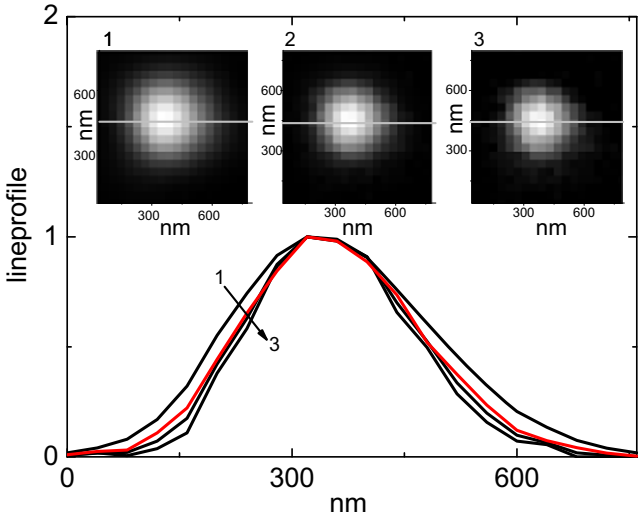

FIGURE 6 Fluorescence intensity contribution corresponding to the first (*1*), second (*2*), and third (*3*) powers of the excitation intensity and the corresponding line profiles. The red curve was obtained from two intensity points calculated as a sum of fifty low- and fifty high-intensity points. The halfwidths (Gaussian fitted) of the line profiles shown are 260 nm (*1*), 210 nm (*2*), 195 nm (*3*), 220 nm (*red*).

only. To have similar amounts of photons from both intensity levels, signal for the low-intensity point with no saturation was acquired for a longer time than that for the high-intensity point with pronounced saturation. Fig. 7 shows the image of a yeast cell with GFP-labeled Ato1p protein, a membrane protein supposed to be an ammonium exporter (19). It is easily observed that the protein is inhomogenously distributed within the membrane by the marked regions where pearl-like structures appear at higher resolution.

Besides the resolution increase, as also shown by line profiles in Fig. 7, another advantage of our imaging method becomes visible when looking into the cell. Whereas the original image exhibits a high autofluorescence signal from the cytosol, the higher-resolution image shows almost the same intensity inside as well as outside the cell. The reason is that most autofluorescent molecules have a much lower extinction coefficient than good fluorescent labels and therefore are much less saturated than, e.g., GFP molecules, which suppresses their contribution in the higher-resolution image.

The important issue that needs to be addressed concerning our approach is the relatively long acquisition time (~11 min in the case of Fig. 7). The most important parameters of the measurement that are involved are the on and off times. In our experiment, we can increase the on time by applying more 80-ps pulses, one after another, with a delay of tens of nanoseconds, which keeps the character of the S_0-to-S_1 saturation and is not enough to recover the molecules that turned into the triplet state. In such a case, we would obtain more photons during the on time, but the triplet-state fraction would increase and more photobleaching would occur as a consequence. In all of the experiments presented here, to prevent any observable photodegradation, we used only one 80-ps pulse. Although the length of the on time can be tuned so that the number of photons within the one on/off period increases and photobleaching is still kept on an acceptable level, the length of the off time is always given by the lifetime of the triplet state. In the presence of oxygen, which is known to be a rather potent triplet quencher, the lifetime of the triplet is usually only a few microseconds; therefore, the length of the dark period has to be 10–20 μs for the system to recover before another excitation takes place. If the recovery is not sufficient, photobleaching would occur due to accumulated molecules in the reactive triplet state and the system would then continue its recovery during the following excitation, and the saturation curve at each pixel would depend on the entire history of the system, which would be far too complex.

One way to shorten the acquisition time is to employ reducing and oxidizing agents (ROXS) (20), possibly together with the removal of oxygen. ROXS quickly reduce/oxidize the triplet state and consequently oxidize/reduce the formed radical anion/cation, thus quenching molecules in the triplet state and repopulating the ground state. The main advantage of using ROXS is its fast depletion of the

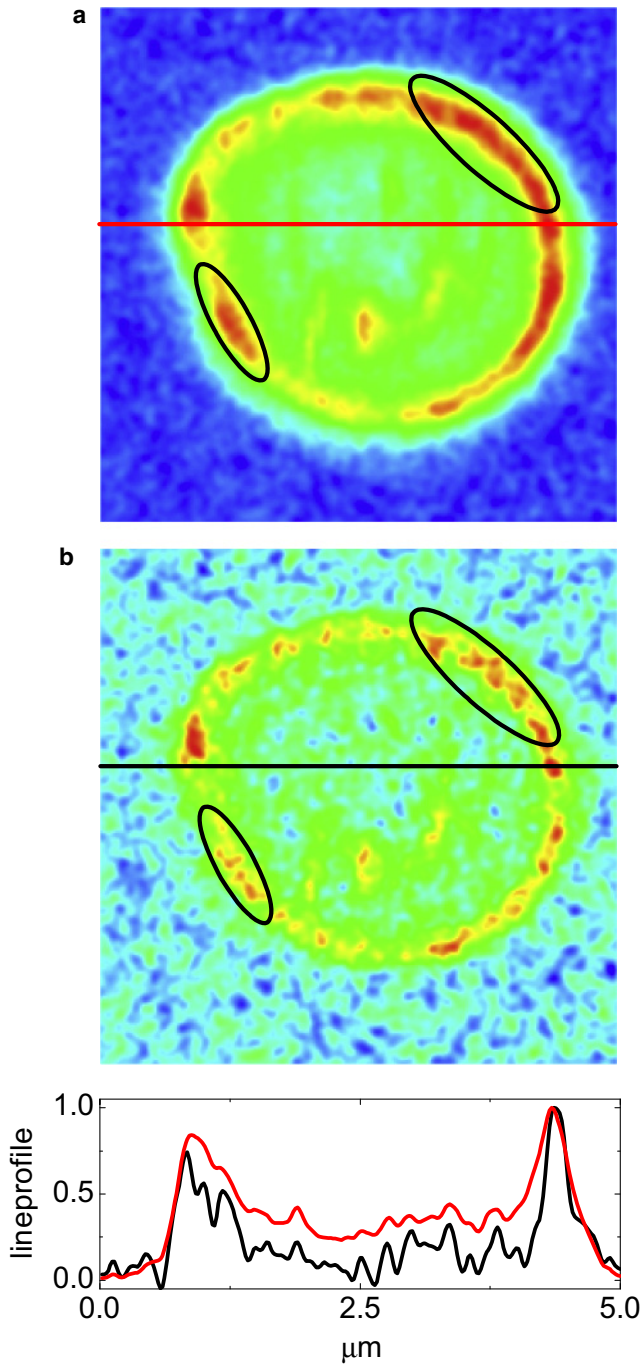

FIGURE 7 Yeast cell with GFP-labeled Ato1p membrane protein. (*a*) Conventional confocal image. (*b*) Fluorescence image corresponding to the second power of the excitation intensity. The image was calculated from two intensity points. The low- and high-intensity points were integrated from 760 and 95 laser pulses, respectively. Pulses were separated by 10 μs (see Fig. 1 *b*). The time spent on one pixel was 10 ms. The image size is 250 $\times$ 250 pixels, with a pixel size of 20 nm. The entire acquisition time was ~11 min. The low-intensity/high-intensity pulse ratio for excitation photons was ~0.2. In the case of the high-intensity pulses, the laser power was 15 μW at 10 MHz at the back aperture of the objective.

triplet state, which almost switches off the most significant photobleaching pathway. This would be helpful when increasing the on time, since the dark state promptly formed from the triplet state is much less reactive. Conversely, the lifetime of the dark state is usually rather long, and the concentrations of the ROXS have to be usually in the millimolar range to reduce the lifetime of the dark state to the microsecond level (20). In summary, using ROXS can reduce the acquisition time or increase the data quality because the on time can be prolonged more easily and not so many on/off cycles are needed. The drawback of employing ROXS would be a loss of universal applicability of our method with respect to the dye, especially as use of ROXS together with fluorescence proteins has never been reported, to the best of our knowledge.

CONCLUSION

In this article, we have described a simple method for resolution enhancement in fluorescence microscopy that is based on the optical saturation of fluorescence in a confocal microscope. It has to be pointed out that our approach works on the same principle as so-called SAX microscopy. The difference between the two methods is analogous to the difference between measuring fluorescence lifetime in frequency (phase fluorometry) and measuring it in the time domain (time-correlated single-photon counting). Both phase fluorometry and SAX use harmonically modulated excitation intensity to observe either the phase shift caused by a delayed fluorescence response or higher-order harmonics caused by the nonlinear dependence of fluorescence intensity on excitation intensity. The time-domain lifetime approaches, as well as the application of the saturation ramp, measure the temporal or excitation intensity dependence of the fluorescence directly and subsequently fit the data to the theoretical model. Although both SAX and the saturation ramp approach provide similar resolution, the latter allows for combining saturation measurements with the so-called T-rex method that enables considerable suppression of photobleaching, which plays a crucial role when high excitation intensities are required. We applied our method to the imaging of fluorescently labeled living yeast cells and were able to show that, in addition to achieving higher image resolution, we could efficiently suppress autofluorescence originating from less saturable molecules.

Compared to the other techniques commonly used to overcome the diffraction limit, the resolution improvement using our approach is rather moderate: our data demonstrate a squeezing of the point-spread function by ~30%. However, since there is no theoretical limit, there is a potential to improve this value by achieving a better signal/noise ratio. Moreover, our method exploits only saturation of the transition between the S_0 and S_1 states, which is achievable for any chromophore. In addition, the method enhances the lateral and axial resolution to a similar extent and causes almost

no photobleaching or degradation of the sample due to long, high-intensity exposures. Last but not least, the need for experimental equipment and further mathematical treatment of the data obtained using our method is rather low.

We thank Dita Strachotová and Aleš Holoubek (Department of Genetics and Microbiology, Faculty of Science of Charles University, Prague, Czech Republic) for providing us with samples of the yeast cells with expressed GFP-labeled Ato1p membrane protein. Finally, we thank Martin Hof for careful reading of the manuscript.

The authors acknowledge financial support from the Academy of Sciences of the Czech Republic (grant KJB400400904 to A.B.), the Ministry of Education of the Czech Republic (grant LC06063 to J.H.), and the Human Frontier Science Program (RGP46/2006 to J.E.) and the German Federal Ministry of Education and Research (FKZ 13N9236 to J.E.).

REFERENCES

1. Hell, S. W., and J. Wichmann. 1994. Breaking the diffraction resolution limit by stimulated emission: stimulated-emission-depletion fluorescence microscopy. *Opt. Lett.* 19:780–782.
2. Donnert, G., J. Keller, R. Medda, M. A. Andrei, S. O. Rizzoli, et al. 2006. Macromolecular-scale resolution in biological fluorescence microscopy. *Proc. Natl. Acad. Sci. USA.* 103:11440–11445.
3. Dyba, M., J. Keller, and S. W. Hell. 2005. Phase filter enhanced STED-4Pi fluorescence microscopy: theory and experiment. *New J. Phys.* 7:134.
4. Wildanger, D., E. Rittweger, L. Kastrup, and S. W. Hell. 2008. STED microscopy with a supercontinuum laser source. *Opt. Express.* 16:9614–9621.
5. Rust, M. J., M. Bates, and X. W. Zhuang. 2006. Sub-diffraction-limit imaging by stochastic optical reconstruction microscopy (STORM). *Nat. Methods.* 3:793–795.
6. Huang, B., W. Q. Wang, M. Bates, and X. W. Zhuang. 2008. Three-dimensional super-resolution imaging by stochastic optical reconstruction microscopy. *Science.* 319:810–813.
7. Bates, M., B. Huang, G. T. Dempsey, and X. W. Zhuang. 2007. Multicolor super-resolution imaging with photo-switchable fluorescent probes. *Science.* 317:1749–1753.
8. van de Linde, S., R. Kasper, M. Heilemann, and M. Sauer. 2008. Photo-switching microscopy with standard fluorophores. *Appl. Phys. B.* 93:725–731.
9. Heilemann, M., S. van de Linde, M. Schuttpelz, R. Kasper, B. Seefeldt, et al. 2008. Subdiffraction-resolution fluorescence imaging with conventional fluorescent probes. *Angew. Chem. Int. Ed.* 47:6172–6176.
10. Gustafsson, M. G. L. 2005. Nonlinear structured-illumination microscopy: wide-field fluorescence imaging with theoretically unlimited resolution. *Proc. Natl. Acad. Sci. USA.* 102:13081–13086.
11. Heintzmann, R., T. M. Jovin, and C. Cremer. 2002. Saturated patterned excitation microscopy: a concept for optical resolution improvement. *J. Opt. Soc. Am. A Opt. Image Sci. Vis.* 19:1599–1609.
12. Fujita, K., M. Kobayashi, S. Kawano, M. Yamanaka, and S. Kawata. 2007. High-resolution confocal microscopy by saturated excitation of fluorescence. *Phys. Rev. Lett.* 99:228105.
13. Yamanaka, M., S. Kawano, K. Fujita, N. I. Smith, and S. Kawata. 2008. Beyond the diffraction-limit biological imaging by saturated excitation microscopy. *J. Biomed. Opt.* 13:050507.
14. Donnert, G., C. Eggeling, and S. W. Hell. 2007. Major signal increase in fluorescence microscopy through dark-state relaxation. *Nat. Methods.* 4:81–86.
15. Donnert, G., C. Eggeling, and S. W. Hell. 2009. Triplet-relaxation microscopy with bunched pulsed excitation. *Photochem. Photobiol. Sci.* 8:481–485.
16. Wach, A. 1996. PCR-synthesis of marker cassettes with long flanking homology regions for gene disruptions in *S. cerevisiae*. *Yeast.* 12:259–265.
17. Sheff, M. A., and K. S. Thorn. 2004. Optimized cassettes for fluorescent protein tagging in *Saccharomyces cerevisiae*. *Yeast.* 21:661–670.
18. Gietz, R. D., R. H. Schiestl, A. R. Willems, and R. A. Woods. 1995. Studies on the transformation of intact yeast cells by the LiAc/SS-DNA/PEG procedure. *Yeast.* 11:355–360.
19. Palkova, Z., F. Devaux, M. Ricicova, L. Minarikova, S. Le Crom, et al. 2002. Ammonia pulses and metabolic oscillations guide yeast colony development. *Mol. Biol. Cell.* 13:3901–3914.
20. Vogelsang, J., R. Kasper, C. Steinhauer, B. Person, M. Heilemann, et al. 2008. A reducing and oxidizing system minimizes photobleaching and blinking of fluorescent dyes. *Angew. Chem. Int. Ed.* 47:5465–5469.